



## Article

# Analysis of Mudstone Fracture and Precursory Characteristics after Corrosion of Acidic Solution Based on Dissipative Strain Energy

Xu Dong <sup>1</sup>, Yu Wu <sup>2,\*</sup>, Kewang Cao <sup>2,3,\*</sup>, Naseer Muhammad Khan <sup>4</sup> , Sajjad Hussain <sup>5</sup> , Seungyeon Lee <sup>6</sup> and Chuan Ma <sup>6</sup>

<sup>1</sup> School of Architecture Engineering, Xuzhou College of Industrial Technology, Xuzhou 221140, China; dongx@mail.xzcit.cn

<sup>2</sup> State Key Laboratory for Geomechanics & Deep Underground Engineering, China University of Mining and Technology, Xuzhou 221116, China

<sup>3</sup> School of Management Science and Engineering, Anhui University of Finance and Economics, Bengbu 233030, China

<sup>4</sup> Department of Mining Engineering, Balochistan University of Information Technology Engineering and Management Sciences, Quetta 87300, Pakistan; engrnaseer1@gmail.com

<sup>5</sup> Department of Mining Engineering, University of Engineering & Technology, Peshawar 25000, Pakistan; engr.sajjad@uetpeshawar.edu.pk

<sup>6</sup> School of Civil, Environmental and Architectural Engineering, Korea University, 145 Anam-ro, Seongbuk-gu, Seoul 02841, Korea; syeon6297@korea.ac.kr (S.L.); machuan94@korea.ac.kr (C.M.)

\* Correspondence: wuyu@cumt.edu.cn (Y.W.); tb18220001b0@cumt.edu.cn (K.C.)



**Citation:** Dong, X.; Wu, Y.; Cao, K.; Muhammad Khan, N.; Hussain, S.; Lee, S.; Ma, C. Analysis of Mudstone Fracture and Precursory Characteristics after Corrosion of Acidic Solution Based on Dissipative Strain Energy. *Sustainability* **2021**, *13*, 4478. <https://doi.org/10.3390/su13084478>

Academic Editor:  
Alberto-Jesus Perea-Moreno

Received: 11 March 2021

Accepted: 14 April 2021

Published: 16 April 2021

**Publisher's Note:** MDPI stays neutral with regard to jurisdictional claims in published maps and institutional affiliations.



**Copyright:** © 2021 by the authors. Licensee MDPI, Basel, Switzerland. This article is an open access article distributed under the terms and conditions of the Creative Commons Attribution (CC BY) license (<https://creativecommons.org/licenses/by/4.0/>).

**Abstract:** The deformation and failure of rock materials are closely related to the strain energy characteristics during the loading process. These strain energy characteristics and rock properties are greatly affected when the rock is subjected to the acidic solution. To study the effects of chemical solutions with different pH on the mechanical properties and strain energy mechanism of mudstone, the chemical corrosion mudstone samples are subjected to a uniaxial loading testing machine (CN64 electro-hydraulic servo). The corrosive effects of the acidic solution on the porosity, strain energy characteristics, and failure mode of mudstone samples were thoroughly investigated. The findings of this research indicate that: (1) The rate of change in the porosity and chemical damage coefficient of rock samples after chemical corrosion decreases, which is closely linear with the increase of solution pH; (2) The total strain energy, elastic strain energy, and dissipative strain energy decrease with the increase of pH, and, as a result, it is proposed that the observed turning point of the proportion curve of dissipated strain energy from decline to rise is used as a precursor point of the rock failure; (3) The stress value of the failure precursor point increases and the strain value decreases with the increase in pH value. However, the ratio of the stress value of the failure precursor point to the peak stress hardly changes with pH value, and its value is about 0.883; and (4) Rock samples soaked in a weak acidic chemical solution (pH 7.3 and 5.3) are damaged by tensile crack, while rock samples soaked in a strong acidic chemical solution (pH 3.3 and 1.3) are mainly damaged by the combination of tensile and shear. The findings of this study can be used to provide an experimental and theoretical foundation for monitoring rock engineering disasters such as slope, tunnel, and coal mine failures.

**Keywords:** strain energy; mudstone; fracture; precursor; acid solution

## 1. Introduction

The strain energy characteristics during the loading process are intimately related to the deformation and failure of rock materials. Furthermore, since the dissipative strain energy and elastic strain energy increase and are released during the loading process, the rock failure usually occurs according to the energy perspective [1,2]. According to the law of thermodynamics, the process of strain energy dissipation is unidirectional and

irreversible. The release of elastic strain energy is bidirectional and reversible under certain conditions. The dissipation of strain energy causes micro-damages to rocks, which weaken their mechanical properties, and especially their macro strength. Internally, rock failure occurs due to the release of elastic strain energy [2,3]. Therefore, the study of the energy variations and their relationship to rock strength and failure during loading can help to reflect the strength change and the nature of rock failure during the loading and fracturing process. This research field has attracted wide attention in academic and engineering circles and has achieved many research results [4–15].

In mining engineering, hydrochemical solutions are common and have a significant impact on the physical and mechanical properties of rocks [16–18]. On the one hand, a hydrochemical solution acts as a lubricant for the rock particles, reducing the friction and bonding forces between them, and thereby the rocks' strength. On the other hand, the hydrochemical solution can react with the minerals and cement within the rock, altering the microstructure and microscopic composition of the rock, and, as a result, the rock's strain energy characteristics [19–21]. Therefore, the impact of hydrochemical solutions on rocks' mechanical properties should be considered not only in terms of the mechanical properties but also of the strain energy characteristics after corrosion. As a result, it is essential to examine the effect of hydrochemical solutions on rocks' mechanical properties and strain energy characteristics from both a theoretical and an engineering perspective.

In recent years, Tang et al. [22] found that the mechanical effect of hydrochemical solutions on rock is closely related to the water-rock chemical action. The main factors affecting the chemical damage of rock are related to the physical properties of rock, the mineral composition, the chemical properties of a solution, the microstructure of a rock, and the non-uniformity of the spatial distribution of material composition. Feng et al. [23] studied the crack propagation characteristics of rock after chemical corrosion. They found that when two prefabricated cracks were connected, the strength of the specimen reached the maximum, the width of coalescence crack increased rapidly when the crack was initiated, and the change of crack velocity characterized the whole process of crack from polymerization, generation, and propagation to failure. Wang et al. [24] found that different chemical solutions had different effects on the mechanical properties of red sandstone. Ionic composition and pH value have a great influence on the mechanical properties of sandstone, and the peak strength, residual strength, and elastic modulus of the rock after corrosion by various chemical solutions decreases to different degrees. Ding et al. [25] designed a limestone dissolution kinetics experiment under different chemical solutions and different times. It was found that the effects of salt and iso-ionic have a great influence on the limestone dissolution rate and rock strength. The salt effect increased the limestone dissolution rate, while the iso-ionic effect decreased the limestone dissolution rate. Han et al. [20,26] studied the damage degradation mechanism and mechanical properties of sandstone specimens under the coupling effect of different chemical solutions and rapid freeze-thaw cycles. It was found that different chemical solutions had different effects on the freeze-thaw damage of sandstone specimens. The  $\text{SO}_4^{2-}$  ion had a greater effect on the freeze-thaw damage than the  $\text{HCO}_3^-$  ion. The hydrochemical solution and freeze-thaw cycle promote each other in the process of sandstone deterioration and affect the degree to which sandstone is damaged. Ma et al. [27–30] analyzed the influence of water on the corrosion seepage characteristics of rock particles, studied the variation characteristics of cracks under the action of pore water pressure, and found that, with the erosion seepage process, the porosity and permeability of all rock samples increased, but the non-Darcy factor decreased. The pore pressure can promote the propagation of the tensile crack, but it inhibits the development of a shear crack. The Kruger model is used to predict the evolution characteristics of permeability based on pores. Miao et al. [31] carried out uniaxial loading rock experiments after corrosion in different pH solutions and found that the corrosive hydrochemical environment has a certain influence on the physical and mechanical properties of rock. The interaction process of various factors is very complex. The chemical reaction and mechanism of water-rock interaction depend on the

specific coupling of the chemical solution's composition with the rock's mineral composition, particles, pores, and fractures. The initial pH value of an acidic solution is a key factor in the degree of rock damage.

The research conducted so far by different scholars has enriched the theory of rock hydrochemical corrosion, as seen in the above review. However, there are few experimental studies on the strain energy characteristics of rock after chemical corrosion. The strength properties, deformation properties, and strain energy mechanism of rock are severely affected by the degradation of physical and mechanical properties of rock caused by chemical solution corrosion. Therefore, it is necessary to study the mechanical and strain energy characteristics of rock after chemical corrosion. In view of the above, this research study discusses the law of water-rock interaction, analyzes the failure process of mudstone samples after chemical corrosion under uniaxial loading from the perspective of strain energy, and puts forward a new method to determine the precursors of rock failure. The findings of this study can be used to provide an experimental and theoretical foundation for monitoring rock engineering disasters such as slope, tunnel, and coal mine failures.

## 2. Experimental Design

### 2.1. Sample Preparation

A representative sample in the form of a boulder was taken from a coal mine in the province of Shandong. All boulder samples were extracted from the working face of the mine. After the extraction of the boulders, the samples were subjected to the stone processing plant for further processing. In this experimental study, a representative sample with a rectangular shape and  $50 \times 50 \times 100$  mm was prepared and used. The edges and side surface were polished with sandpaper to make it smooth and keep the parallelism error of both ends less than 0.2 mm. To dry rock samples, the rock samples were placed in the drying oven and baked for 48 h, and were then sealed and stored in plastic bags for further experiments. Naturally, the ionic composition of the mine water near the coal mining face is complicated. Therefore, it is very challenging to simulate the corrosion impacts of all chemical ionic contents on the rock in the experiment.  $\text{Na}^+$ ,  $\text{K}^+$ , and  $\text{Cl}^-$  are the most common ionic components of mine drainage. Therefore, in this paper, NaCl and KCl were used as the electrolyte solute to customize the chemical solution properly and represent the chemical composition of mine drainage [24]. Furthermore, the rock inside the coal mine interacts mainly with acidic water with a pH value that varies in different regions, but lies mostly in the range of 2.0–6.3. This study mainly configured an acidic solution to study its corrosion effect on mudstone.

When establishing different groups of hydrochemical solutions, it is believed that if the pH value interval is small, there may be no difference between the two neighboring groups of chemical solutions for rock corrosion. As a result, the pH range of the solution should surpass the pH of the water in the mine. Furthermore, it is essential to mention that the interaction between water and rock in mining engineering is a long-term process. To replicate the condition of the mine in a short period, the concentration of the solution needs to be increased. Considering the above three factors, four kinds of acidic solutions, with pH values of 1.3, 3.3, 5.3, and 7.3, were prepared and used in this experiment. NaCl and KCl with a concentration of 0.1 mol/L were used as electrolyte. The details of the chemical solution are shown in Table 1. After the electrolyte solution was prepared, a 68%  $\text{HNO}_3$  solution was added dropwise to achieve the required pH value. The solution was continuously stirred in a glass cup during the addition of 68%  $\text{HNO}_3$  through the dropper to ensure that the solute was fully dissolved and that the ion distribution was uniform. During the preparation of the acid solution, an acid-base pH meter measured the pH of the solution in real-time until the desired pH was reached. Before the experiment, each rock sample was numbered. In this study, a total of 16 rock samples were processed and divided into four groups. The groups were named; A, B, C, and D, and the corresponding pH values of acid solution were 1.3, 3.3, 5.3, and 7.3, respectively. The rock samples of groups A, B, C, and D are numbered  $A_1, \dots, A_4, B_1, \dots, B_4, C_1, \dots, C_4$ , and  $D_1, \dots, D_4$ .

respectively. Due to the inevitable discreteness of the rock mechanics experiment, in order to weaken the influence of discreteness on the experimental results to a certain extent, rock samples whose peak strength deviated from the maximum average value in each group were removed. Three rock samples were left in each group, and the total of 12 rock samples was used for the subsequent data analysis and statistics. After numbering, each group of rock samples was immersed in 2 L of the prepared chemical solution. During the soaking process, the pH of the solution was monitored by an acid-base pH meter, and the weight change of the rock sample was recorded. The pH value and the weight change of rock samples were recorded every two hours in the early stage of immersion, and once in a day when the pH value of a solution changed slightly.

**Table 1.** Preparation of chemical solutions.

	<b>Solution Composition</b>	<b>Solution Concentration/(Mol/L)</b>	<b>pH</b>
Neutral solution	NaCl, KCl	0.1	7.3
Acid solution	NaCl, KCl	0.1	5.3
Acid solution	NaCl, KCl	0.1	3.3
Acid solution	NaCl, KCl	0.1	1.3

## 2.2. Experimental Equipment and Methods

The experiment's findings revealed that a solution of pH 3.3 and 5.3 achieved pH 7 in 30 days, suggesting that the chemical reaction of  $H^+$  in the solution was virtually complete in 30 days. Therefore, all rock samples in this analysis were soaked in a chemical solution for 30 days. Mine water and rock interact in a semi-open space environment during mining operations. Hence, this experiment implemented a semi-open soaking state in the soaking of rock samples. The semi-open soaking means that the mudstone is completely immersed in a vessel containing an acid solution, but the top of the vessel is not covered, that is, the solution is connected with the outside air during the soaking process, which enables the soaking process to take place in the presence of natural air, which will truly reflect the water-rock chemical reaction in a mining environment. During the soaking period, the solvent is often mixed in a glass cup to ensure that the ions in the solution thoroughly react with the soaked rock.

The MTS CN64.106 electro-hydraulic servo universal testing machine manufactured by MTS Pressure System Company in the United States was used for the uniaxial loading control system. The maximum capacity of uniaxial loading is 1000 kN, the force and displacement precision is  $\pm 0.5\%$ , and the frequency of data collection is 1–50 times per second. In this article, the chemical corroded mudstone was subjected to a uniaxial loading unit at equivalent displacement. The loading rate was 0.1 mm/min, and the duration of the press acquisition of data was set to 10 times per second [32,33].

## 3. Experimental Results

### 3.1. Water–Rock Interaction

#### 3.1.1. pH Value

The variation of pH value of the chemical solution during the mudstone soaking process is shown in Figure 1. This revealed that, during the soaking interval 0–102 h, the pH value of the solution increased quickly from 5.3 to 6.7. The rise in the pH value of the solution in the soaking interval 102–432 h was marginally quicker than the soaking interval 0–102 h, and the pH value rose from 6.7 to 7.2 and then steadily increased. In the soaking process interval, 432–600 h, only a 0.5 increase was noticed, and the solution pH reached 7.7 at 600 h. The pH value was 7.7 at a soaking period of 600 h and remained unchanged until the end of the soaking process. Similarly, for a solution with pH = 3.3, the pH increased from 3.3 to 5.4, during a soaking process in the interval 0–156 h. The pH value of the solution in a soaking process in the interval 156–504 h rose significantly slower than that in the soaking interval 0–156 h. In this interval, the pH value increased from 5.4 to

7.1. The pH value of the solution increased very slowly after 504 h to the end of the soaking process, and its pH value at the end of the process was 7.4. During the soaking process, the pH value increased to 7.3 at 600 h and 384 h in a solution with pH values of 3.3 and 5.3, respectively. This increase indicates that the  $H^+$  in the solution had completely reacted with rock minerals at this interval time, and then the pH value continued to rise. This is because there are alkaline minerals in the mineral composition of mudstone. The same can be confirmed by the pH transition of the solution with pH = 7.3. The authors found that the solution with pH = 7.3 rose slowly to 7.7 and remained unchanged. The solution with pH = 1.3 remained nearly constant throughout the mudstone soaking process, and the pH value was just 1.5 until the end of the soaking process. This is due to the solution with pH = 1.3 having a high concentration and high  $H^+$  content, and the chemical reaction with mudstone minerals absorbing a limited amount of  $H^+$ .

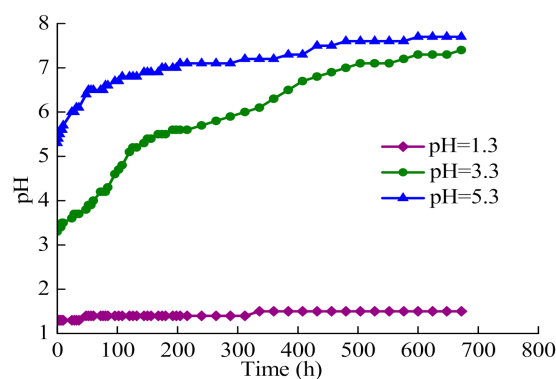


**Figure 1.** Changes of pH value of the solution with soaking time.

### 3.1.2. Porosity

Mudstone is a type of soft rock, which has more main pores and microfractures than sandstone. The porosity assessment formula is as follows [20]:

$$n = \left(1 - \frac{\rho_g}{\rho}\right) \times 100\% \quad (1)$$

where  $n$  is the porosity of mudstone,  $\rho_g$  is the bulk density, and  $\rho$  is the particle density.

Table 2 shows the initial porosity, the porosity change rate after chemical solution corrosion, and the damage parameter of mudstone. The trend between the average porosity change rate and pH is shown in Figure 2. The porosity change rate of rock samples decreases nearly linear with the increase of pH. The porosity change rates of groups A, B, C, and D are 7.77%, 6.27%, 4.38%, and 1.89%, respectively. The porosity change rate of group A is 4.11 times that of group D, the one in group B is 3.32 times that of group D, and the one in group C is 2.32 times that of group D. Acidity has a significant impact on the porosity of rocks, and with the rise of acidity, the degradation of rocks becomes more evident. Note that group D is a neutral solution, and, after acid solution corrosion, the porosity change rate is 1.89%. The reason is that, after soaking in a neutral solution, the dissolution of water on the soluble minerals, such as some chlorides and some oxides (iron, aluminum oxides, etc.) in the rock allows the porosity of the rock to increase. The increase in porosity of groups A, B, and C is due to the chemical reaction of  $H^+$  with mudstone feldspar, calcite, and mica, and the resulting materials slowly overflow with an immersed solution. This overflow of material causes an increase in rock porosity. It is evident, from the microscopic point of view, that the shape and mineral composition of mudstone has improved due to chemical solution. The damage caused by chemical solution corrosion to mudstone is mainly due to the dissolution of soluble cement and the chemical reaction with its mineral composition. This reaction causes changes in the microstructure of mudstone, continuously forming damage, and finally resulting in the weakening of the mechanical properties. In

this paper, the damage variable of porosity is used to define the corrosion damage degree of chemical solution corrosion to the mudstone specimen. The chemical damage parameter  $D_{ch}$  was calculated as follows [26]:

$$D_{ch} = 1 - \frac{1 - n_t}{1 - n_0} \quad (2)$$

where  $n_t$  is the porosity of the mudstone after chemical corrosion, and  $n_0$  is the initial porosity of the mudstone.

**Table 2.** Porosity and porosity change rate of mudstone before and after immersion in a chemical solution.

Number	Initial Porosity/%	Porosity After Corrosion/%	Chemical Damage Parameters/%
A <sub>1</sub>	15.74	16.95	1.44
A <sub>2</sub>	16.01	17.24	1.47
A <sub>3</sub>	15.88	17.14	1.50
B <sub>1</sub>	16.33	17.38	1.25
B <sub>2</sub>	15.92	16.92	1.19
B <sub>3</sub>	16.04	17.02	1.17
C <sub>1</sub>	16.21	16.93	0.85
C <sub>2</sub>	15.85	16.56	0.84
C <sub>3</sub>	16.08	16.76	0.81
D <sub>1</sub>	15.77	16.07	0.36
D <sub>2</sub>	15.80	16.12	0.38
D <sub>3</sub>	16.17	16.45	0.33

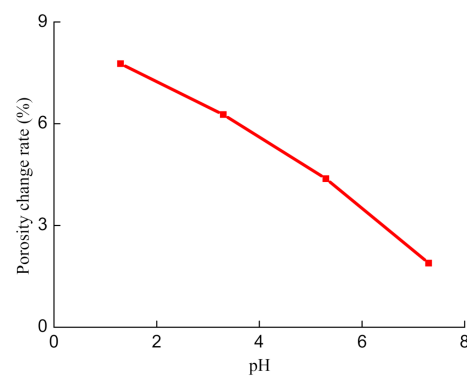


**Figure 2.** Variation of porosity with solution pH.

The volume density of mudstone was calculated as follows:

$$\rho_g = \rho_v \times \frac{m_0}{m_1 - m_2} \quad (3)$$

where,

- $m_0$ —mass of dry mudstone (g)
- $m_1$ —mass of saturated mudstone (g)
- $m_2$ —mass of saturated mudstone in water (g)
- $\rho_v$ —density of water (g/cm<sup>3</sup>)

The dry rock sample was first weighed while measuring the initial porosity of the mudstone sample, and then the rock was soaked in water to saturation state, and the mass

in air and water was measured. Finally, in order to make dry rock samples, all rock samples were baked for 48 h in the oven. The particle density was calculated as follows:

$$\rho = \rho_V \times \frac{m_3}{m_4 + m_3 - m_5} \quad (4)$$

where

- $m_3$ —Mass of dry rock sample powder (g)
- $m_4$ —Mass of a density bottle containing distilled water (g)
- $m_5$ —Mass of a density bottle containing rock sample powder and distilled water (g)

In the calculation of particle density, three parts of rock powder were made, respectively, and the average value of particle density was taken as the particle density of mudstone selected in this paper.

The microstructure and mineral composition of the mudstone samples have changed to different degrees after corrosion by an aqueous chemical solution. This change caused chemical damage to the samples, which decreased their macro mechanical parameters. The chemical damage variable  $D_{ch}$  of the mudstone sample after corrosion in the acid solution was determined using Equation (3), and the relationship between  $D_{ch}$  and pH was obtained as shown in Figure 3. The average value of the chemical damage variable  $D_{ch}$  was taken from each rock sample group, and the pattern of variance of the chemical damage variable was drawn at the pH level. The rate of porosity change in rock samples decreased almost linearly with the rise in pH, as shown in Figure 3. After soaking in acidic solution, the chemical damage  $D_{ch}$  of groups A, B, C, and D was 1.47%, 1.21%, 0.83%, and 0.36%, respectively. The chemical damage variable  $D_{ch}$  of group A was 4.08 times that of group D, the one in group B was 3.36 times that of group D, and the one in group C was 2.31 times that of group D.

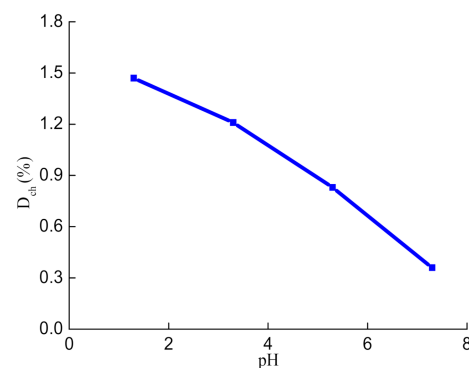


**Figure 3.** Variation of chemical damage coefficient with solution pH.

## 4. Strain Energy

### 4.1. The Calculation of Strain Energy

Rocks deform under the action of loading. It is assumed that the uniaxial loading process of a rock takes place in a closed system without heat exchange with the surrounding environment, in which case the following formula can be obtained:

$$U = U^d + U^e \quad (5)$$

where  $U$  is the total strain energy,  $U^d$  is the dissipative strain energy, and  $U^e$  is the elastic strain energy.

Figure 4 shows the relationship between the dissipated strain energy and the elastic strain energy during uniaxial loading of rock. As shown in Figure 4, the total strain energy

is the area under the stress-strain curve, which is OBC. The formula of total strain energy in uniaxial loading of rock is as follows:

$$U = \int_0^{\varepsilon} \sigma d\varepsilon \quad (6)$$

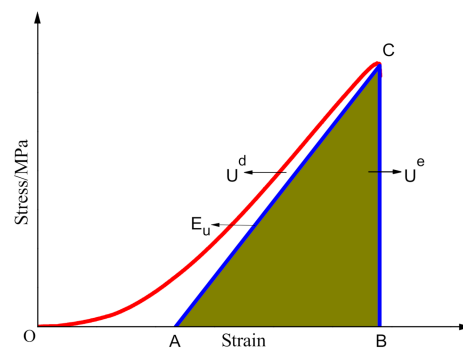


**Figure 4.** The elastic strain energy and dissipative strain energy curve of rock during uniaxial loading.

The elastic strain energy is the area of the shaded part in Figure 4, which is ABC. The elastic strain energy of rock under uniaxial loading is calculated as follows

$$U^e = \frac{1}{2E_u} \sigma^2 \quad (7)$$

where the slope of AC ( $E_u$ ) is the unloading modulus of elasticity.

The dissipated strain energy is the area under OAC in Figure 4. The calculation formula is as follows:

$$U^d = U - U^e = \int_0^{\varepsilon} \sigma d\varepsilon - \frac{1}{2E_u} \sigma^2 \quad (8)$$

For the convenience of calculation, the unloading elastic modulus ( $E_u$ ) is usually replaced by the elastic modulus ( $E$ ). The elastic modulus is calculated by taking two points in the straight section of the stress-strain curve and calculating the slope. Mathematically, it can be calculated as:

$$E = \frac{f(\varepsilon_2) - f(\varepsilon_1)}{\varepsilon_2 - \varepsilon_1} \quad (9)$$

#### 4.2. Strain Energy Characteristics

Figure 5 shows the strain energy evolution curve of rock samples corroded by different pH acid solutions during loading. The total strain energy increased the stress-strain curve in the compaction, elastic, and plastic stage. In the compaction stage, the total strain energy increased slowly with the increase of strain, as shown in Figure 5. The total strain energy is the sum of elastic and dissipation energy. The dissipative strain energy increase is higher than that of elastic strain energy. In this stage, dissipative strain energy is consumed by the compaction of primary pores and microcracks. In the elastic stage, the input energy provided by the loading is mainly used for the elastic deformation of the internal structure of the rock sample and is mainly converted into elastic strain energy storage, while the dissipated strain energy is almost unchanged or slightly increased. In the plastic stage, the input energy provided by loading is still mainly stored in the form of elastic strain energy. However, due to a large number of new meso cracks in the rock, the dissipated strain energy increases greatly near the peak strength, due to propagation and connection of meso cracks and macro cracks formed in the sample. After the peak strength, a large amount of elastic strain energy stored in the rock is released rapidly, while the dissipated strain



energy increases rapidly. A large amount of dissipated strain energy is dissipated by plastic deformation, macro crack penetration, and slip dislocation of macro crack surface, and the rock strength gradually loses energy. The same trends of accumulation, transformation, and damage mechanism were observed for different groups. However, the difference in pH of the chemical solution will inevitably lead to the obvious difference of strain energy value at peak strength. Table 3 describes the statistics of total strain energy, elastic strain energy, and dissipated strain energy at the peak strength points of all rock samples. In order to intuitively reflect the influence of the pH value of the chemical solution on the strain energy value of the rock samples at a peak strength point, the strain energy value of each group of rock samples at peak strength point was taken, and the average value was calculated. The histogram is drawn as shown in Figure 6. The average values of total strain energy of A, B, C and D are 0.1046 g/cm<sup>3</sup>, 0.1008 g/cm<sup>3</sup>, 0.009544 g/cm<sup>3</sup>, and 0.08574 g/cm<sup>3</sup>, respectively. The average values of elastic strain energy are 0.06461 g/cm<sup>3</sup>, 0.06612 g/cm<sup>3</sup>, 0.07113 g/cm<sup>3</sup>, and 0.06148 g/cm<sup>3</sup>, respectively. The average values of dissipated strain energy are 0.03994 g/cm<sup>3</sup>, 0.03472 g/cm<sup>3</sup>, 0.02431 g/cm<sup>3</sup>, and 0.02426 g/cm<sup>3</sup>, respectively. The total strain energy at the peak strength point decreases with the increase of pH, the elastic strain energy first increases and then decreases with the increase of pH, and the dissipative strain energy decreases with the increase of pH. However, low acidity (pH 5.3 and 7.3) shows a slight effect on the dissipative strain energy at the peak strength point. This conclusion can also be verified from the failure patterns of the rock samples below. The dissipated strain energy is mainly used for rock damage and fracture development. When pH is 5.3 and 7.3, the failure patterns of rock samples are mainly a tensile failure, and there are few secondary microcracks on the surface.

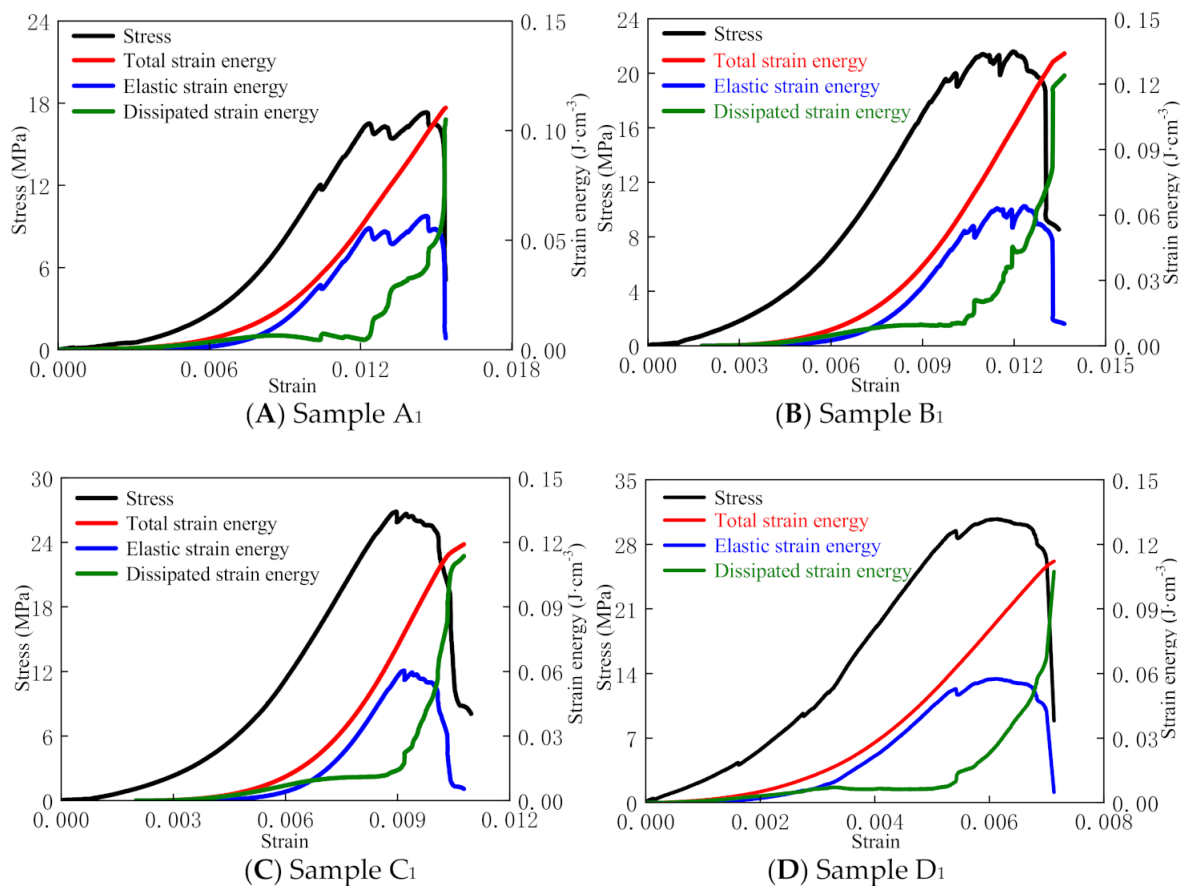
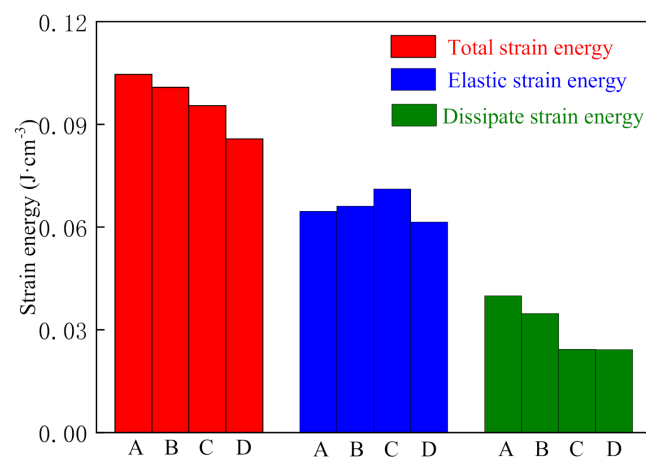


Figure 5. Strain energy evolution curve of rock samples during uniaxial loading.

**Table 3.** Strain energy value of the peak stress point of rock samples after chemical corrosion.

Number	Total Strain Energy/g·cm <sup>3</sup>	Elastic Strain Energy/g·cm <sup>3</sup>	Dissipative Strain Energy/g·cm <sup>3</sup>
A <sub>1</sub>	0.0979	0.0557	0.0422
A <sub>2</sub>	0.112	0.0735	0.0389
A <sub>3</sub>	0.103	0.0647	0.0387
B <sub>1</sub>	0.0888	0.0541	0.0347
B <sub>2</sub>	0.0914	0.0633	0.0282
B <sub>3</sub>	0.0880	0.0691	0.0189
C <sub>1</sub>	0.0777	0.0605	0.0172
C <sub>2</sub>	0.0871	0.0711	0.0159
C <sub>3</sub>	0.0728	0.0603	0.0394
D <sub>1</sub>	0.0633	0.0357	0.0276
D <sub>2</sub>	0.0881	0.0696	0.0184
D <sub>3</sub>	0.0530	0.0420	0.0110

**Figure 6.** Histogram of strain energy at the peak point of rock samples after chemical solution corrosion.

### 5. The Precursor of Rock Failure

The energy transformation of rock from deformation to failure is a complicated mechanism, that illustrates the conversion and equilibrium between the total strain energy input, elastic strain energy, and dissipative strain energy. Dissipative strain energy is the essence of rock fracture and failure. The increase in dissipative strain energy during uniaxial loading causes internal damage, resulting in the degradation and loss of rock strength. The change in dissipative strain energy can be used to represent the loaded rock's damage characteristics. The failure instability of rock can be monitored more accurately if the dissipation strain energy is used to evaluate the fracture and failure characteristics of the rock. The ratio of dissipated strain energy refers to the ratio of dissipated strain energy to total strain energy. The rocks soaked in different pH chemical solutions show the variation trend of the proportion of dissipated strain energy with time during uniaxial loading, as shown in Figure 7. The ratio of dissipation strain energy curve shows a downward trend before the peak stress, and it turns to increase before the peak strength. The dissipated strain energy curve continues to increase until the rock failure occurs, as shown in Figure 7. The curve of the ratio of the dissipated strain energy increases abruptly when the rock failure occurs. It was found that all the curves of the ratio of the dissipated strain energy went through the process of “descending-ascending” when the rock samples were near to failure. The reason is that, when the rock is near failure, internal microcracks develop rapidly, and dissipated strain energy is gradually used for the propagation of plastic strain and crack. While the elastic strain energy still accumulates, the rock approaches the limit of

energy conservation. Therefore, from declining to increasing, the ratio of dissipated strain energy increases, and thus the elastic strain energy exceeds the energy storage limit, and the stored elastic strain energy is rapidly released, resulting in rock failure.

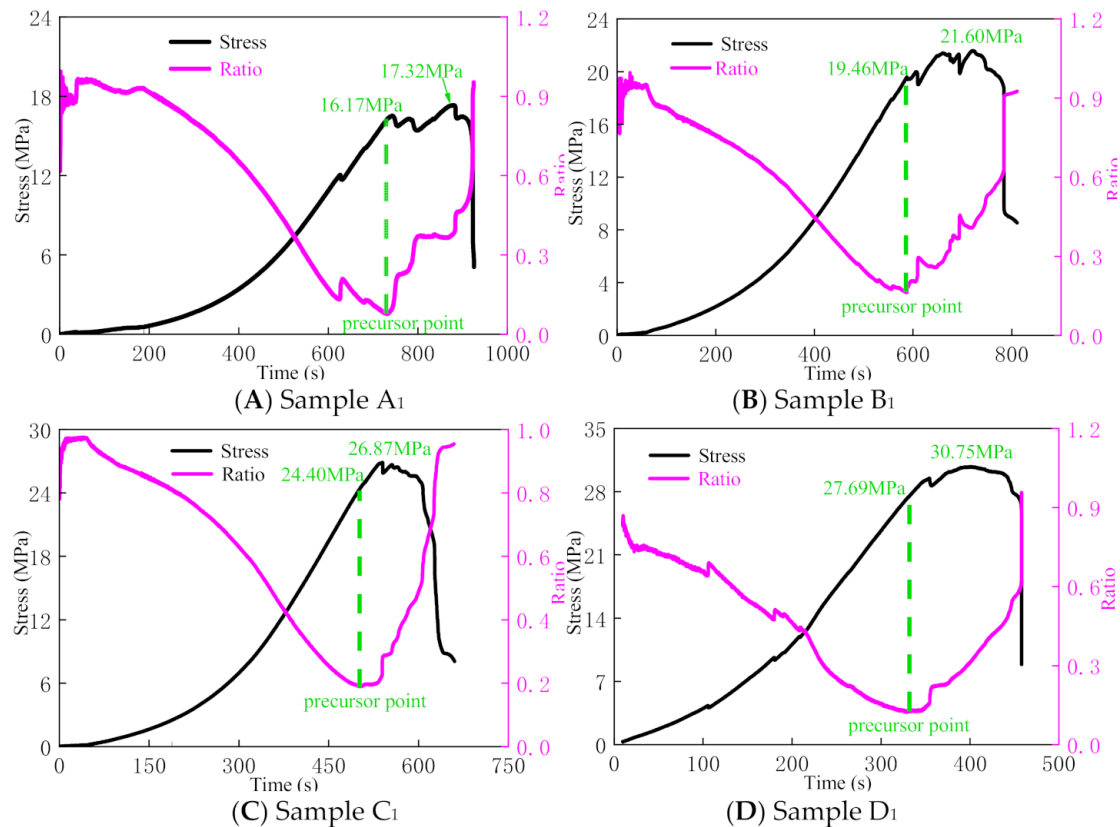


**Figure 7.** The variation curve of dissipated energy ratio with time during uniaxial loading of rock samples.

The authors assume that in the process of rock fracturing, the following three characteristics can be used as a background for evaluating the precursor characteristics of rock based on the strain energy: (1) The precursory characteristics of rock failure should be obvious before rock failure, which is easy to extract quantitatively, and all rock samples have this characteristic; (2) The rock fracture signal, reflected by precursory characteristics, should be fracture produced by high energy release, because energy release is the internal cause of the sudden fracture of a rock. It is easy to track and accurately calibrate the evolution process of rock failure and instability disaster by grasping the strain energy signal generated by fracture type, which plays an important role in the formation and development of rock failure and instability; (3) Select a relatively small number of index change types, as far as possible, for the rock failure's precursor characteristic signal, to reduce false positives and omissions and improve the accuracy of the prediction of rock failure.

In conclusion, the turning point of the ratio curve of dissipated strain energy from decreasing to increasing can be used as the precursor of rock failure. As shown in Figure 7, the stress value at the failure precursor point of rock sample A<sub>1</sub> is 16.17 MPa, the peak strength is 17.32 MPa, and the ratio of the stress value at the precursor point to the peak strength is 0.93. The stress corresponding to the failure precursor of rock sample B<sub>1</sub> is 19.46 MPa, the peak strength is 21.60 MPa, and the ratio of the stress at the precursor point to the peak stress is 0.90. The stress corresponding to the failure precursor of rock sample C<sub>1</sub> is 24.40 MPa, the peak strength is 26.87 MPa, and the ratio of the stress at the precursor point to the peak stress is 0.91. The stress value corresponding to the failure precursor of rock sample D<sub>1</sub> is 27.69 MPa, the peak strength is 30.75 MPa, and the ratio of the stress value at the precursor point to the peak stress is 0.90. Table 4 shows the stress and strain

values at the failure precursor point, the stress and strain values at the peak point, and the ratio of the stress and strain values at the precursor point to the stress and strain values at the peak point. The stress value of the failure precursor points increases nearly linearly, while the strain value of the failure precursor points decreases nearly linearly, as shown in Figures 8 and 9, with the increase of pH. Moreover, as the pH of the solution increases by 1, the stress value increases by about 2.18 MPa, while the strain value decreases by about 0.00123. The linear equation can be used to determine the stress and strain values of the failure precursor point in various acidic solutions.

**Table 4.** The stress and strain values of rock samples at the failure precursor point and peak stress point.

Number	Precursor Point (A)		Peak Point		Ratio	
	Stress/MPa	Strain	Stress/MPa	Strain	$\sigma_A/\sigma_{max}$	$\epsilon_A/\epsilon_{max}$
A <sub>1</sub>	16.17	0.0120	17.33	0.0146	0.933	0.822
A <sub>2</sub>	15.58	0.0151	18.61	0.0177	0.837	0.853
A <sub>3</sub>	13.53	0.0119	17.51	0.0153	0.773	0.778
B <sub>1</sub>	19.47	0.00965	21.59	0.0119	0.902	0.811
B <sub>2</sub>	17.30	0.0101	21.54	0.0118	0.803	0.856
B <sub>3</sub>	20.28	0.0113	22.11	0.0123	0.917	0.919
C <sub>1</sub>	24.40	0.00833	26.87	0.00896	0.908	0.929
C <sub>2</sub>	25.58	0.00854	27.01	0.0090	0.947	0.949
C <sub>3</sub>	23.05	0.00688	26.25	0.00896	0.878	0.768
D <sub>1</sub>	26.76	0.00506	30.41	0.00613	0.880	0.825
D <sub>2</sub>	29.05	0.00581	31.70	0.00638	0.916	0.911
D <sub>3</sub>	27.69	0.00598	30.77	0.00609	0.900	0.982

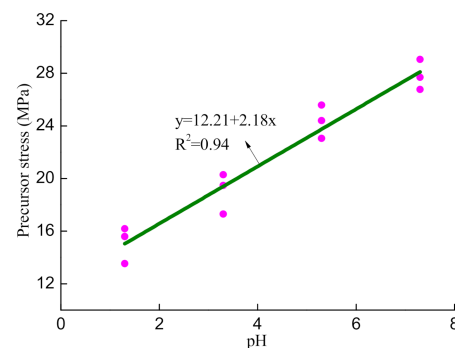


**Figure 8.** The variation curve of stress value at the failure precursor point of rock samples with solution pH.

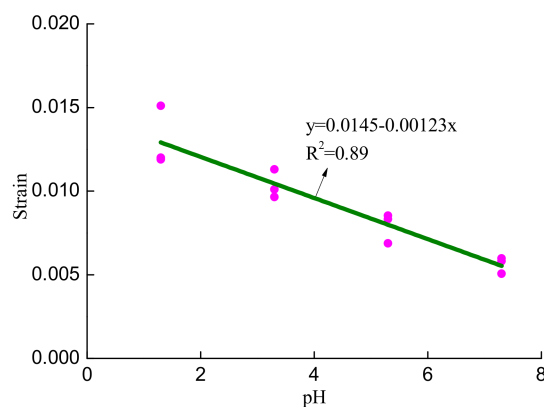


**Figure 9.** The variation curve of strain value of the rock samples' failure precursor point with solution pH.

According to Table 4, assess the mean value of each group of rock samples and draw the histogram to evaluate the changing pattern with the pH solution as shown in Figure 10. The ratio of strain to peak strain at the failure precursor point increases with the rise of the pH solution, while the stress to peak stress ratio at the failure precursor point first increases and then decreases. The ratios of the stress value at the failure precursor point to the peak stress of the rock samples of groups A, B, C, and D were 0.848, 0.874, 0.911, and 0.899, respectively. The ratios of the stress value at the failure precursor point to the peak stress of rock samples soaked in different pH acid solutions had little variance, first rising and then decreasing with an increase in pH. Therefore, the authors attempted to use a straight line to fit the ratio of the stress value at the failure precursor point and peak stress of mudstone after soaking in acidic solutions with different pH values. As shown in Figure 11, the ratio of the stress value at the failure precursor point to the peak stress is about 0.883, and there is no obvious relationship between the ratio and the pH value of the solution. Therefore, the rock failure precursor point can be evaluated by testing the uniaxial compressive strength of mudstone, and the evolution state of rock strain energy can be distinguished. When the stress value reaches the rock failure precursor point, the curve of the proportion of the rock's dissipative strain energy has reached the lowest point, and then the dissipative strain energy will increase rapidly. The crack and fissure will generate and propagate rapidly, and rock failure will occur soon.

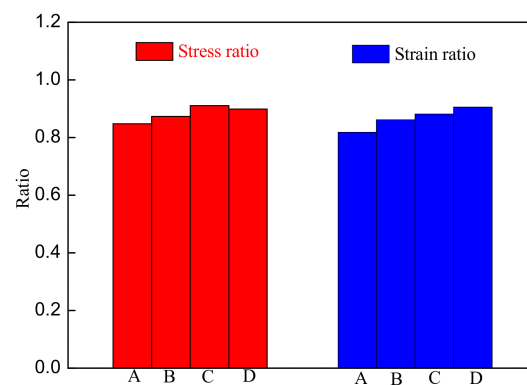


Figure 10. The ratio of stress-strain at the failure precursor point to stress-strain at the peak point.

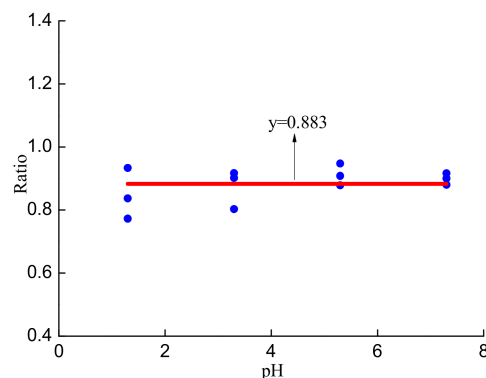
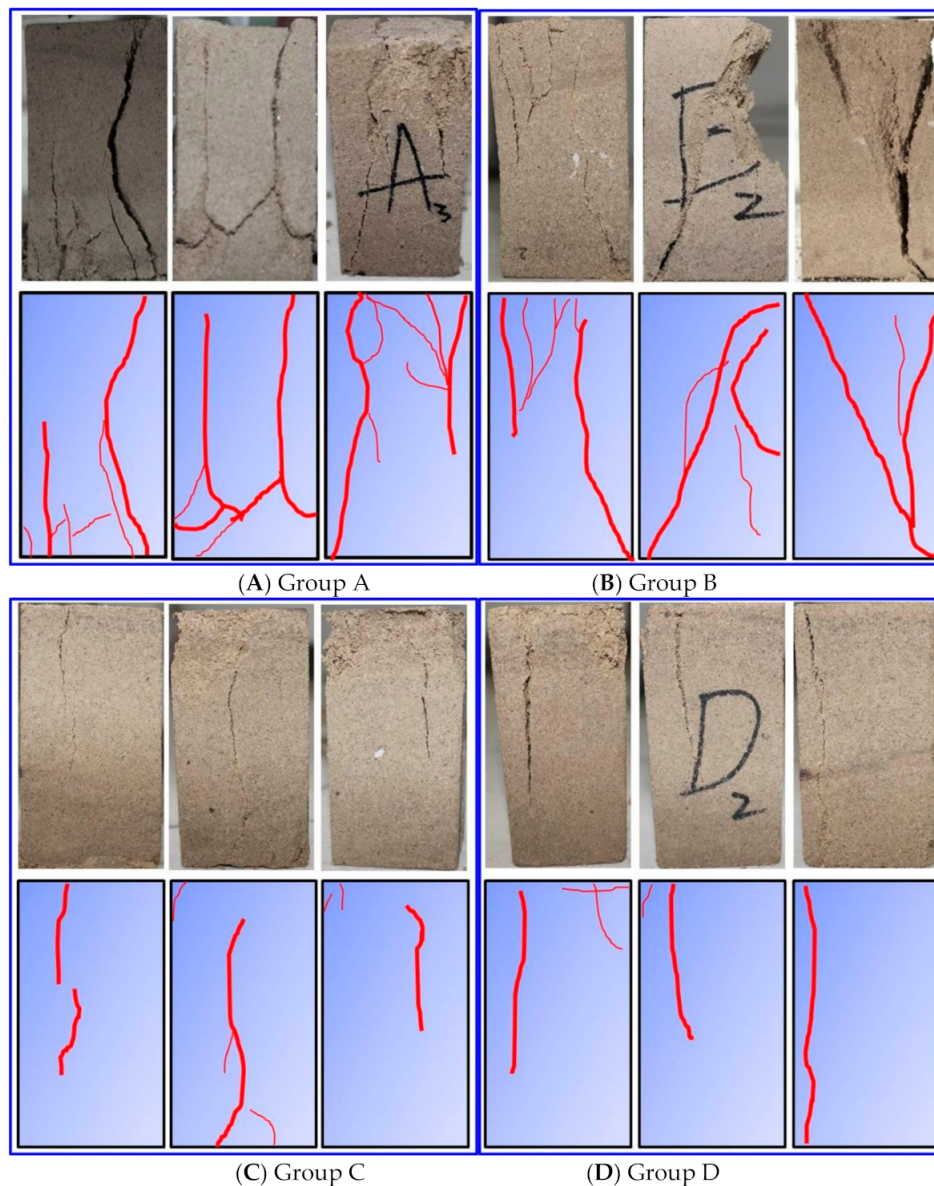


Figure 11. The variation trend of the ratio of precursory stress to peak stress with pH.

## 6. Failure Mode

The above study indicates that the strain energy value at the peak point of mudstone and the stress and strain at the failure precursor point change with the change in the pH value of the chemical solution. Therefore, the authors infer that the failure mode of mudstone can also change with the change in the pH value of the chemical solution under uniaxial loading. The failure mode of mudstone corroded by acid solutions with different pH values under uniaxial loading was photographed, and the crack propagation

pattern was sketched and analyzed. Figure 12 shows the failure pattern sketch of mudstone corroded by acid solutions with different pH values under uniaxial loading. The failure mode under uniaxial loading of rock samples corroded by weak acidic solution (pH 7.3 and 5.3) is a tensile crack failure, and a few secondary microcracks appear in some rock samples, as shown in Figure 12. The failure mode under uniaxial loading of rock samples corroded by a strong acid solution (pH = 3.3 and 1.3) is predominantly in the form of a tensile scissor combination. There are visible tensile or shearing main cracks and several shears and tensile bifurcation cracks on the rock surface. It is concluded that the mudstone failure pattern appears to be complicated by the increased acidity of the solution and that the number of secondary microcracks after rock failure increases.



**Figure 12.** The failure mode and a sketch of rock samples under uniaxial loading after chemical corrosion.

The content of  $H^+$  is higher in a stronger acidic solution than a weak acidic solution. This has a strong corrosion effect on mudstone. The porosity change rate of mudstone is significantly higher than that of a weak acidic solution. Meanwhile, the peak strain and the dissipated strain energy at the peak point increase with the increase in acidity. Due to the equal displacement loading method used in this experiment, the increase of peak strain will

lead to an increase in the duration of the rock fracture development stage. It can be seen from the above that the stress value of the failure precursor point decreases with solution acidity. Therefore, mudstone begins to fail, and crack propagation occurs irregularly at a lower stress level. In addition, the increase in porosity also promotes the development and propagation of microcracks. In view of the strain energy, the crack development of mudstone is the result of the increase of dissipated strain energy. Due to this increase of the dissipated strain energy at the peak point, more microcracks will appear in the plastic stage, the load-carrying capacity of the particles will be weakened after sliding, the damage before the peak stress and the internal crack propagation will be intensified, and nucleation and penetration will occur when the dissipated strain energy increases rapidly. As a result, the number of microcracks is large, and their shape is complex. To summarize, the porosity, peak strain, and dissipated strain energy at the peak point of mudstone corroded by the strong acid solution are greater than those of the weak acid solution. The combined action of the three factors results in more micro cracks on the surface of mudstone corroded by a strong acid solution, and the failure state is usually complex.

## 7. Conclusions

The following conclusions were drawn.

- (1) The rate of change in porosity and the coefficient of chemical damage of the rock samples after chemical corrosion decreases almost linearly with an increase in the pH value of the chemical solution.
- (2) The total strain energy, elastic strain energy, and dissipative strain energy at the peak stress point decrease with the increase in the pH value of a chemical solution. It is proposed that the turning point of the ratio curve of dissipated strain energy from decline to rise can be considered as the precursory point of rock failure.
- (3) The stress value increases and the strain value decreases at the failure precursor point with the increase of the pH value of the chemical solution. However, the ratio of the stress value of the failure precursor point to the peak stress slightly changes with the change of the pH value, which is 0.883.
- (4) Rock samples soaked in a weak acidic chemical solution (pH = 7.3 and 5.3) are damaged by a tensile crack, while rock samples soaked in a strong acidic chemical solution (pH = 3.3 and 1.3) are mainly damaged by tensile shear combination.

**Author Contributions:** D.X. contributed to the research experiments and wrote the paper. Y.W. and K.C. conceived this research and were responsible for the research. N.M.K. and S.L. collected and preprocessed the original data. S.H. and C.M. reviewed and revised the paper. C.M. and S.L. helped in polishing the manuscript. All authors have read and agreed to the published version of the manuscript.

**Funding:** This research received no external funding.

**Institutional Review Board Statement:** Not applicable.

**Informed Consent Statement:** Not applicable.

**Data Availability Statement:** Data is contained within the article.

**Acknowledgments:** The authors gratefully acknowledge Qiupeng Yuan for helpful suggestions.

**Conflicts of Interest:** We declare that we do not have any commercial or associative interest that represents a conflict of interest in connection with the work submitted.

## References

1. Xie, H.P.; Ju, Y.; Li, L.Y. Rock strength and global failure criterion based on energy dissipation and release principle. *Chin. J. Rock Mech. Eng.* **2005**, *24*, 3003–3010.
2. Xie, H.P.; Ju, Y.; Li, L.Y.; Peng, R.D. Energy mechanism of deformation and failure process of rock mass. *Chin. J. Rock Mech. Eng.* **2008**, *27*, 1729–1740.

3. Gao, R.; Kuang, T.J.; Zhang, Y.Q.; Zhang, W.Y.; Quan, C.Y. Controlling mine pressure by subjecting high-level hard rock strata to ground fracturing. *Int. J. Coal Sci. Technol.* **2021**. [[CrossRef](#)]
4. Zhang, Y.; Feng, X.T.; Zhang, X.; Wang, Z.; Yang, C. A novel application of strain energy for fracturing process analysis of hard rock under true triaxial compression. *Rock Mech. Rock Eng.* **2019**, *52*, 4257–4272. [[CrossRef](#)]
5. Zhou, Y.; Sheng, Q.; Li, N.; Fu, X.D. The influence of strain rate on the energy characteristics and damage evolution of rock materials under dynamic uniaxial compression. *Rock Mech. Rock Eng.* **2020**, *53*, 3823–3834. [[CrossRef](#)]
6. Zuo, J.P.; Wang, J.T.; Jiang, Y.Q. Macro/meso failure behavior of surrounding rock in deep roadway and its control technology. *Int. J. Coal Sci. Technol.* **2019**, *6*, 301–319. [[CrossRef](#)]
7. Dou, L.T.; Yang, K.; Chi, X.L. Fracture behavior and acoustic emission characteristics of sandstone samples with inclined precracks. *Int. J. Coal Sci. Technol.* **2021**, *8*, 77–87. [[CrossRef](#)]
8. Chen, Y.L.; Zuo, J.P.; Liu, D.J.; Li, Y.J.; Wang, Z.B. Experimental and numerical study of coal-rock bimaterial composite bodies under triaxial compression. *Int. J. Coal Sci. Technol.* **2021**. [[CrossRef](#)]
9. Ding, X.; Xiao, X.C.; Wu, D.; Lv, X.F. Mechanical properties and charge signal characteristics in coal material failure under different loading paths. *Int. J. Coal Sci. Technol.* **2019**, *6*, 138–149. [[CrossRef](#)]
10. Li, Y.; Huang, D.; Li, X.A. Strain rate dependency of coarse crystal marble under uniaxial compression: Strength, deformation and strain energy. *Rock Mech. Rock Eng.* **2014**, *47*, 1153–1164. [[CrossRef](#)]
11. Pan, X.H.; Lu, Q. A quantitative strain energy indicator for predicting the failure of laboratory scale rock samples: Application to shale rock. *Rock Mech. Rock Eng.* **2018**, *51*, 2689–2707. [[CrossRef](#)]
12. Rezaei, M.; Hossaini, M.F.; Majdi, A. Determination of longwall mining induced stress using the strain energy method. *Rock Mech. Rock Eng.* **2015**, *48*, 2421–2433. [[CrossRef](#)]
13. Cai, W.; Dou, L.M.; Si, G.Y.; Cao, A.Y.; Gong, S.Y.; Wang, G.H.; Yuan, S.S. A new seismic-based strain energy methodology for coal burst forecasting in underground coal mines. *Int. J. Rock Mech. Min. Sci.* **2019**, *123*, 104086. [[CrossRef](#)]
14. Feng, P.; Xu, Y.; Dai, F. Effects of dynamic strain rate on the energy dissipation and fragment characteristics of cross-fissured rocks. *Int. J. Rock Mech. Min. Sci.* **2021**, *138*, 104600. [[CrossRef](#)]
15. Zhang, Z.Z.; Deng, M.; Bai, J.B.; Yu, X.Y.; Wu, Q.H.; Jiang, L.S. Strain energy evolution and conversion under triaxial unloading confining pressure tests due to gob-side entry retained. *Int. J. Rock Mech. Min. Sci.* **2020**, *126*, 104184. [[CrossRef](#)]
16. Zhang, K.; Li, H.F.; Han, J.M.; Jiang, B.B.; Gao, J. Understanding of mineral change mechanisms in coal mine groundwater reservoir and their influences on effluent water quality: A experimental study. *Int. J. Coal Sci. Technol.* **2021**, *8*, 154–167. [[CrossRef](#)]
17. Guo, P.Y.; Gu, J.; Su, Y.; Wang, J.; Ding, Z.W. Effect of cyclic wetting-drying on tensile mechanical behavior and microstructure of clay-bearing sandstone. *Int. J. Coal Sci. Technol.* **2021**, 1–13.
18. Yu, H.; Gui, H.R.; Zhao, H.H.; Wang, M.C.; Li, J.; Fang, H.X.; Jiang, Y.Q.; Zhang, Y.R. Hydrochemical characteristics and water quality evaluation of shallow groundwater in Suxian mining area, Huaibei coalfield, China. *Int. J. Coal Sci. Technol.* **2020**, *7*, 1–11. [[CrossRef](#)]
19. Sho, O.; Hideaki, Y.; Naoki, K.; Dae, S.C.; Kiyoshi, K. Modeling of coupled thermal-hydraulic-mechanical-chemical processes for predicting the evolution in permeability and reactive transport behavior within single rock fractures. *Int. J. Rock Mech. Min. Sci.* **2018**, *107*, 271–281.
20. Han, T.; Shi, J.; Cao, X. Fracturing and damage to sandstone under coupling effects of chemical corrosion and freeze–thaw cycles. *Rock Mech. Rock Eng.* **2016**, *49*, 4245–4255. [[CrossRef](#)]
21. Lin, Y.; Gao, F.; Zhou, K.; Gao, R.G. Mechanical properties and statistical damage constitutive model of rock under a coupled chemical-mechanical condition. *Geofluids* **2019**, *2019*, 7349584. [[CrossRef](#)]
22. Tang, L.; Zhang, P.; Wang, S. Experimental study on the macroscopic mechanical effects of water-rock chemistry on rocks. *Chin. J. Rock Mech. Eng.* **2002**, *21*, 526–531.
23. Feng, X.T.; Ding, W.X. Experimental study of limestone micro-fracturing under a coupled stress.; fluid flow and changing chemical environment. *Int. J. Rock Mech. Min. Sci.* **2007**, *44*, 437–448. [[CrossRef](#)]
24. Wang, W.; Li, X.H.; Zhu, Q.Z.; Shi, C.; Xu, W.Y. Experimental study of mechanical characteristics of sandy slate under chemical corrosion. *Rock Soil Mech.* **2017**, *9*, 2559–2566.
25. Ding, W.; Chen, J.; Xu, T.; Chen, H.; Wang, H. Study on mechanical and chemical dissolution characteristics of limestone under chemical solution erosion. *Rock Soil Mech.* **2015**, *36*, 1825–1830.
26. Han, T.; Chen, Y.; Shi, J.; Yu, C.; He, M. Experimental study on the influence of hydrochemical corrosion on mechanical properties of sandstone. *Chin. J. Rock Mech. Eng.* **2013**, *32*, 3065–3072.
27. Ma, D.; Zhang, J.X.; Duan, H.Y.; Huang, Y.L.; Li, M.; Sun, Q.; Zhou, N. Reutilization of gangue wastes in underground backfilling mining: Overburden aquifer protection. *Chemosphere* **2021**, *264*, 128400. [[CrossRef](#)]
28. Ma, D.; Duan, H.Y.; Li, X.B.; Li, Z.H.; Zhou, Z.L.; Li, T.B. Effects of seepage-induced erosion on nonlinear hydraulic properties of broken red sandstones. *Tunn. Undergr. Space Technol.* **2019**, *91*, 102993. [[CrossRef](#)]
29. Ma, D.; Duan, H.Y.; Zhang, Q.; Zhang, J.X.; Li, W.X.; Zhou, Z.L.; Liu, W.T. A numerical gas fracturing model of coupled thermal, flowing and nechanical effects. *Comput. Mater. Contin.* **2020**, *65*, 2123–2141. [[CrossRef](#)]
30. Ma, D.; Duan, H.Y.; Liu, J.F.; Li, X.B.; Zhou, Z.L. The role of gangue on the mitigation of mining-induced hazards and environmental pollution: An experimental investigation. *Sci. Total Environ.* **2019**, *664*, 436–448. [[CrossRef](#)]



31. Miao, S.J.; Cai, M.F.; Guo, Q.F.; Wang, P.T.; Liang, M.C. Damage effects and mechanisms in granite treated with acidic chemical solutions. *Int. J. Rock Mech. Min. Sci.* **2016**, *88*, 77–86. [[CrossRef](#)]
32. Cao, K.; Naseer, K.H.; Liu, W.; Hussain, S.; Zhu, Y.; Cao, Z.; Bian, Y. Prediction model of dilatancy stress based on brittle rock: A case study of sandstone. *Arab. J. Sci. Eng.* **2021**, *46*, 2165–2176. [[CrossRef](#)]
33. Cao, K.W.; Ma, L.; Wu, Y.; Naseer, K.H.; Yang, J. Cyclic fatigue characteristics of rock failure using infrared radiation as precursor to violent failure: Experimental insights from loading and unloading response. *Fatigue Fract. Eng. Mater. Struct.* **2020**, *44*, 584–594. [[CrossRef](#)]